Deep geothermal energy:

A meeting place for rock physics and the energy systems transition

Alexandra R. L. KUSHNIR

28 May 2020

École et observatoire des sciences de la Terre
Université de Strasbourg

IPGS Strasbourg

Enhanced Geothermal Systems (EGS)

Geothermal exploitation mines sub-surface heat for heat and / or electricity production.

Hot water is brought to the surface (via production well) and cold water is pumped down (via injection well), to be heated again.

Permeability of the reservoir is key to production.

How do we maintain reservoir permeability?

In naturally fractured reservoirs, the fractures networks are often sealed or become sealed over time.

Enhanced Geothermal Systems: aim to re-activate these fractures, via chemical or hydraulic stimulation

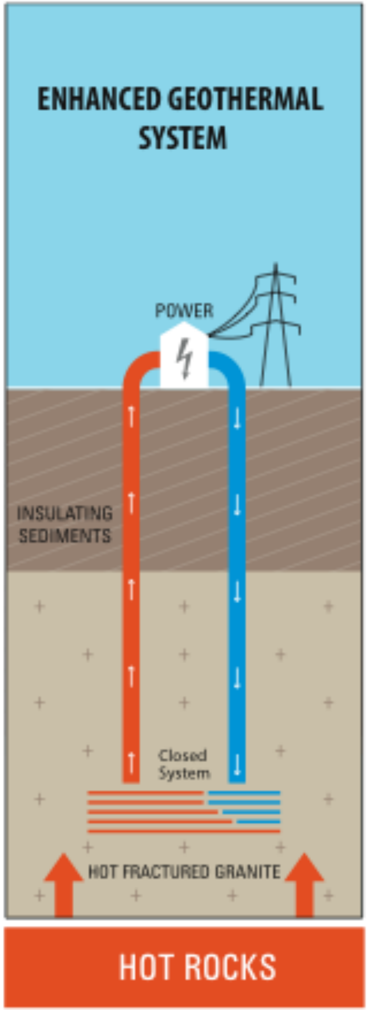

Lostinscience.wordpress.com

EGS and the Upper Rhine Graben

The Upper Rhine Graben hosts thermal anomalies

Soultz-sous-Forêts (France), Rittershoffen (France), Brühl (Germany), Landau (Germany), Insheim (Germany), Bruchsal (Germany), and Riehen (Switzerland)

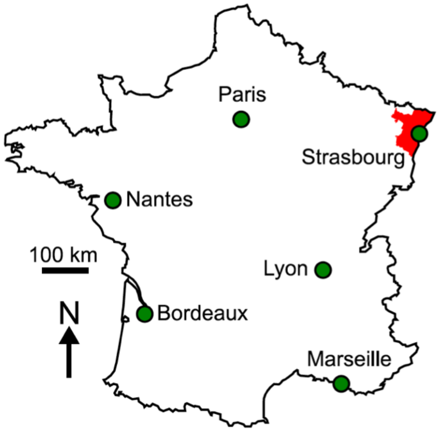

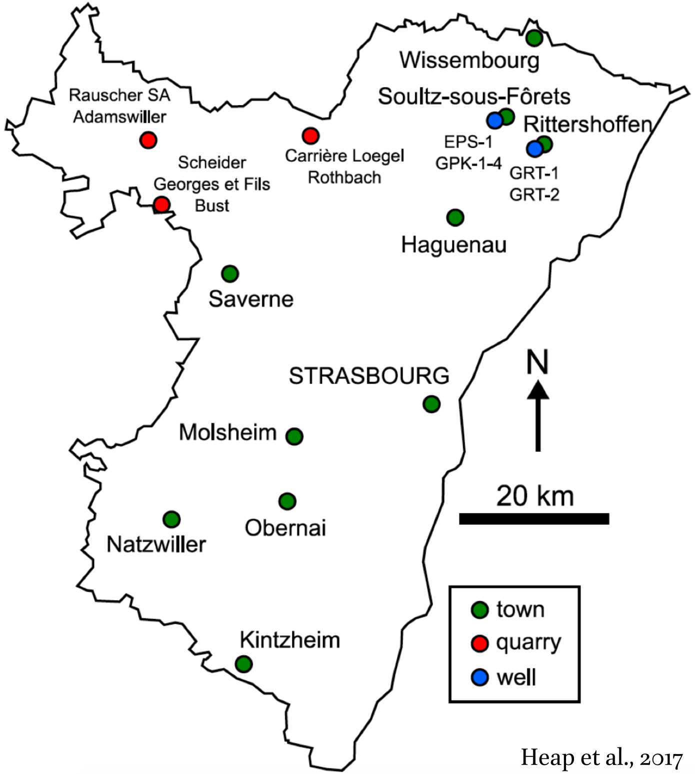

Heap et al., 2017

EGS and the Upper Rhine Graben

The Upper Rhine Graben hosts thermal anomalies

Soultz-sous-Forêts (France), Rittershoffen (France), Brühl (Germany), Landau (Germany), Insheim (Germany), Bruchsal (Germany), and Riehen (Switzerland)

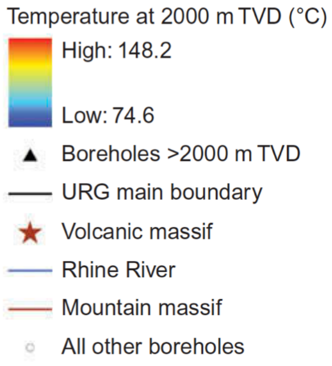

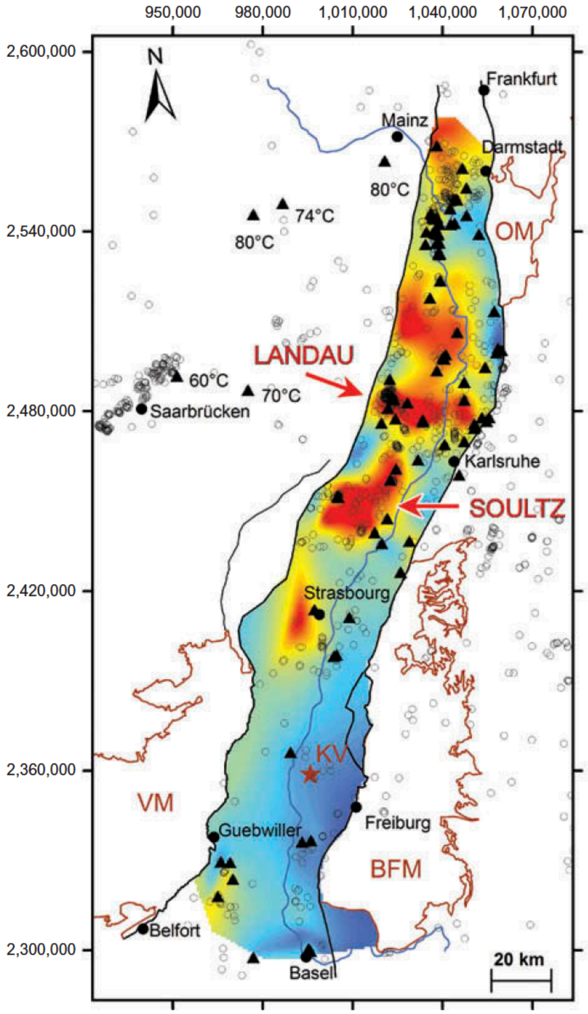

Baillieux et al., 2013

EGS and the Upper Rhine Graben

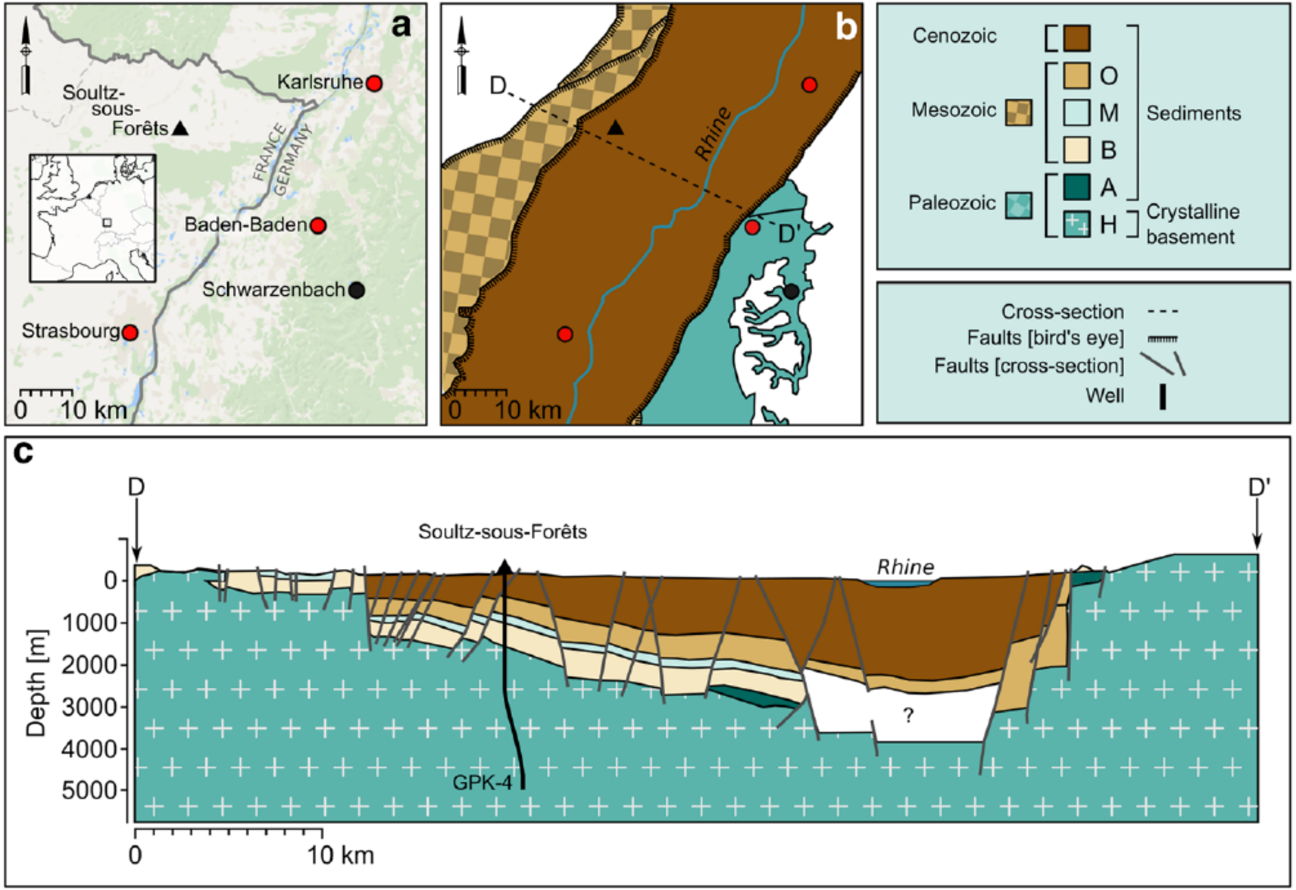

Farquharson et al., 2020

EGS and the Upper Rhine Graben

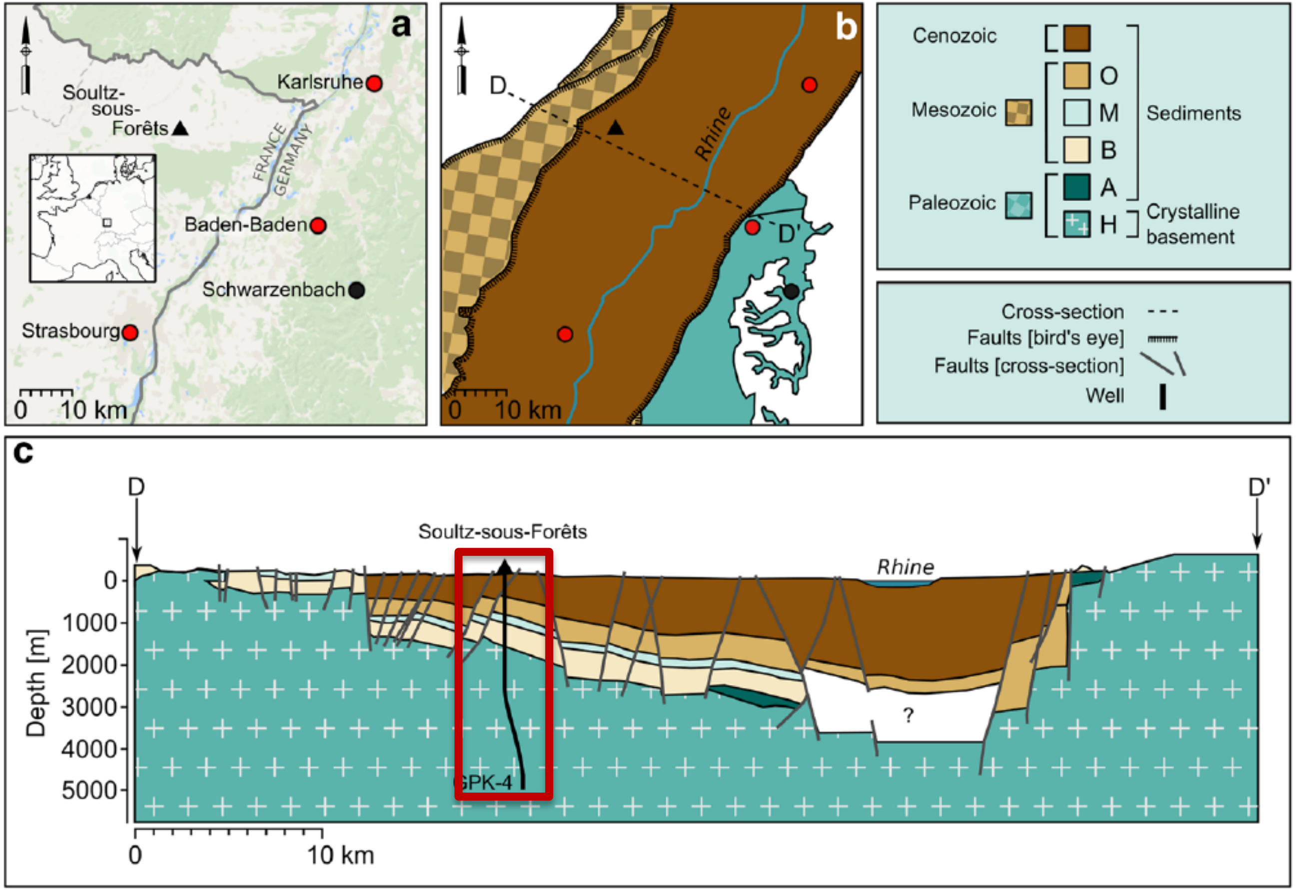

Farquharson et al., 2020

EGS and the Upper Rhine Graben

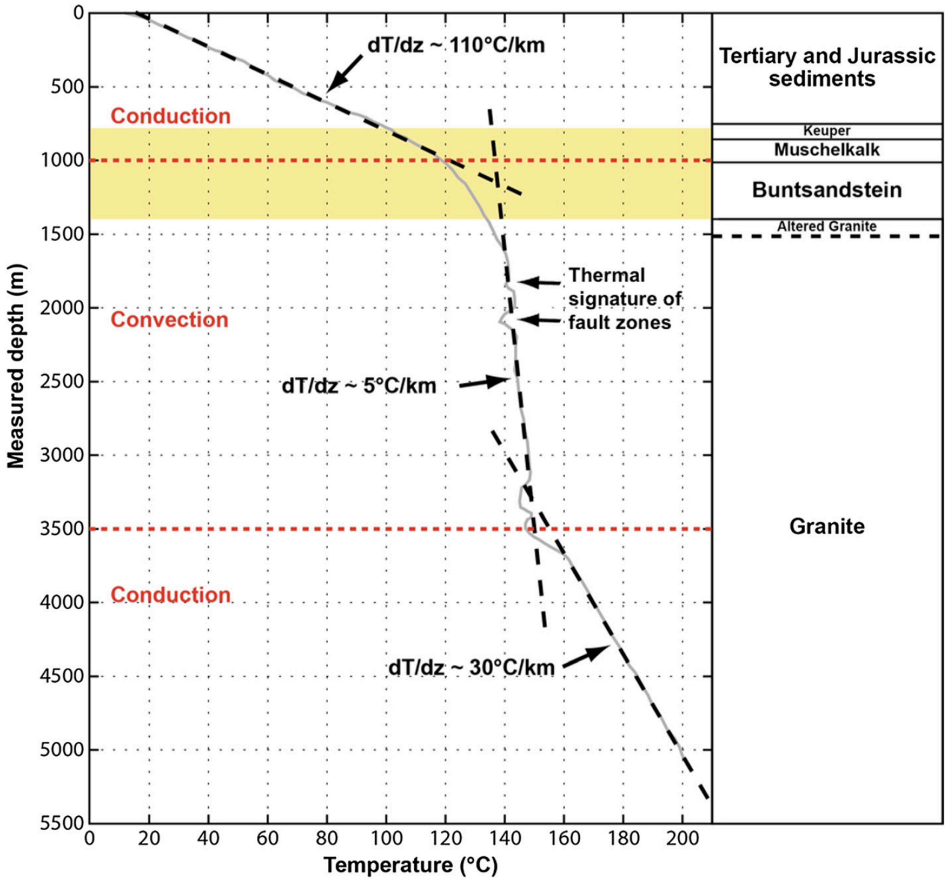

Vidal et al., 2015

Temperature anomaly is due to a convection zone.

The granite reservoir is overlain by sedimentary sequences, notably the buntsandstein and muschelkalk.

Two areas can be targetted for exploitation:

- granite
- granite-buntsandstein transition zone

EGS and the Upper Rhine Graben

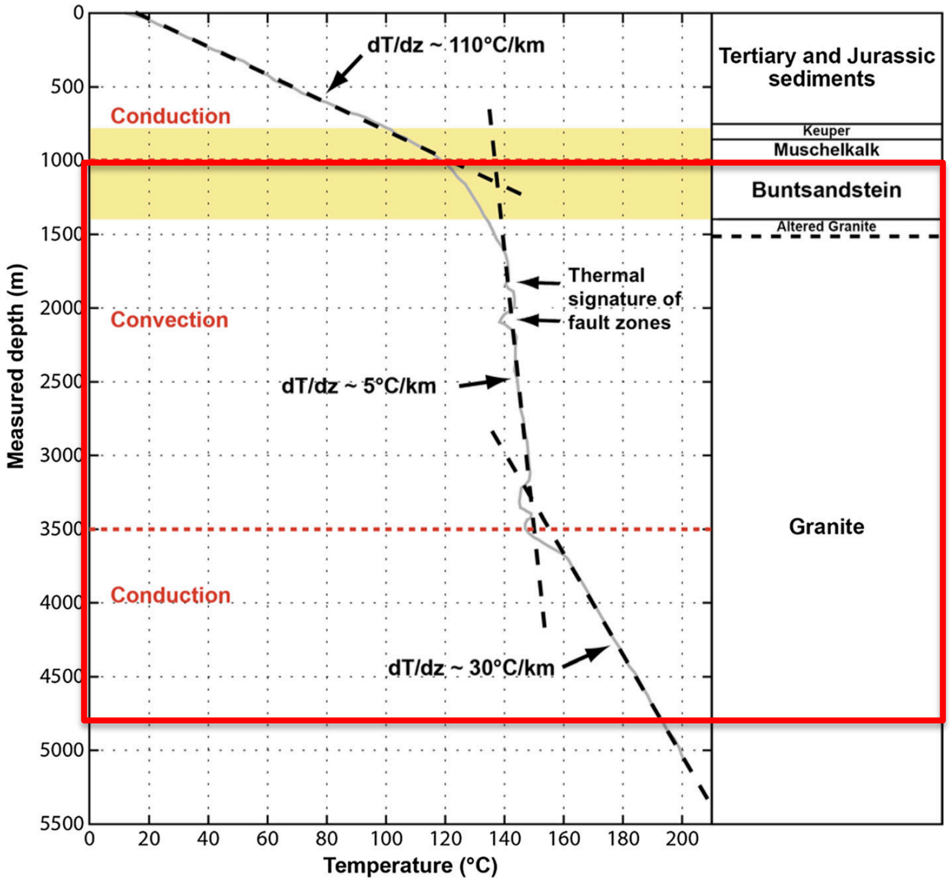

Vidal et al., 2015

Temperature anomaly is due to a convection zone.

The granite reservoir is overlain by sedimentary sequences, notably the buntsandstein and muschelkalk.

Two areas can be targetted for exploitation:

- granite
- granite-buntsandstein transition zone

Soultz-sous-Forêts and the EPS-1 exploration borehole

Vertical hole down to 2227 m

Continuously cored from 930 to 2227 m:
930 – 1000 m – muschelkalk
1000 – 1417 m – buntsandstein
1417 – 2227 m – granite

Core can be matched up with borehole geophysical and televiewer data.

Today we will talk about the buntsandstein and the granite.

In the laboratory

Sample size: tens of millimeters

Rock physical property characterisation:

- **Porosity**
- **Permeability**
- **Seismic wave velocities**
- Rock strength / elastic moduli
- Thermal properties
- Electrical properties

Process-focussed experiments looking into :

- Rock fluid interactions
- Reactivation of pre-existing fractures

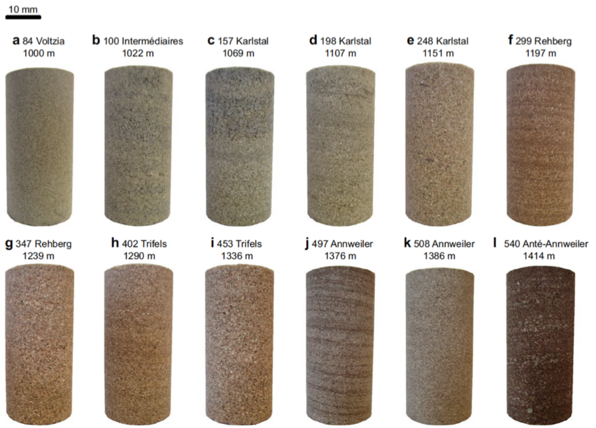

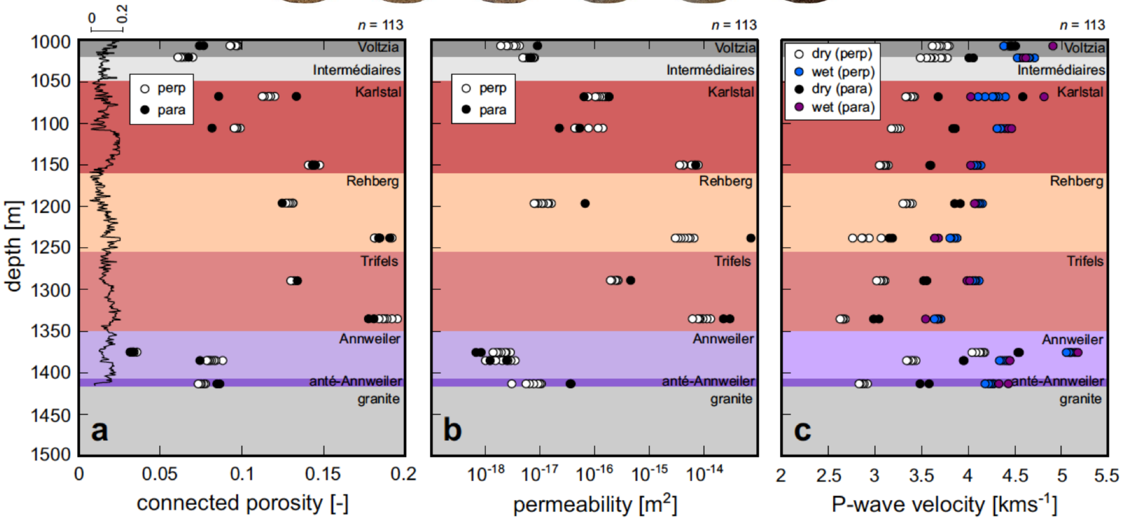

EPS-1 Buntsandstein. Heap et al. 2017

In the laboratory

Sample size: tens of millimeters

Rock physical property characterisation:

- Porosity
- Permeability
- Seismic wave velocities
- **Rock strength / elastic moduli**
- Thermal properties
- Electrical properties

Process-focussed experiments looking into :

- Rock fluid interactions
- Reactivation of pre-existing fractures

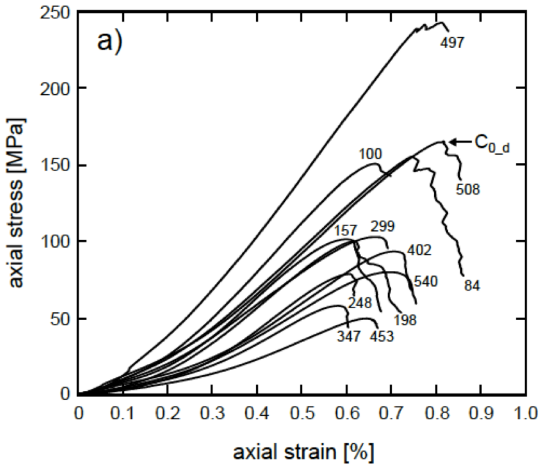

UCS of Buntsandstein

Heap et al. 2019

Sample number	Depth (m)	Presence of phenocrysts	Bulk dry density (kg/m³)	Connected porosity	Confining pressure (MPa)	Compressive strength (MPa)
1	1420	Not noted	2652	0.0030	0	123.6
2	1420	Not noted	2650	0.0029	0	N/A
3	1915	Not noted	2696	0.0018	0	129.2
4	1915	Not noted	2686	0.0018	0	128.4
5	1915	Not noted	2682	0.0020	0	146.9
3A	1558	No	2679	0.0012	0	153.1
6A	1558	No	2658	0.0012	0	144.6
2A	1558	No	2672	0.0012	5	263.0
3C	1558	No	2671	0.0011	10	296.8
4A	1558	No	2678	0.0011	20	369.5
5A	1558	No	2666	0.0012	30	433.3
1A	1558	Yes	2667	0.0012	0	140.6
2C	1558	Yes	2669	0.0012	0	152.4
1C	1558	Yes	2656	0.0011	5	255.9
2B	1558	Yes	2665	0.0009	10	277.2
3B	1558	Yes	2686	0.0011	20	363.3
8B	1558	Yes	2639	0.0016	30	380.6

UCS of Soultz granite

Villeneuve et al. 2018

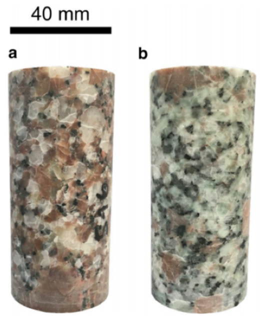

In the laboratory

Sample size: tens of millimeters

Rock physical property characterisation:
- Porosity
- Permeability
- Seismic wave velocities
- Rock strength / Elastic moduli
- Thermal properties
- Electrical properties

Process-focussed experiments looking into :
- **Rock fluid interactions**
- Reactivation of pre-existing fractures

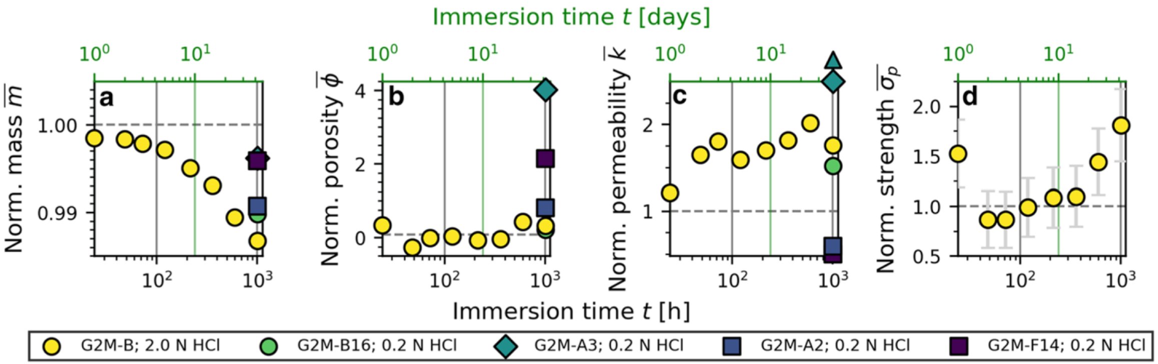

Physical property evolution in granite as a function of time, when immersed in HCl.
Farquharson et al. 2020

In the laboratory

Sample size: tens of millimeters

Rock physical property characterisation:

- Porosity
- Permeability
- Seismic wave velocities
- Rock strength / Elastic moduli
- Thermal properties
- Electrical properties

Process-focussed experiments looking into :

- Rock fluid interactions
- Reactivation of pre-existing fractures

117
Moderately-sealed joint

179
Poorly-sealed joint

388
Well-sealed joint

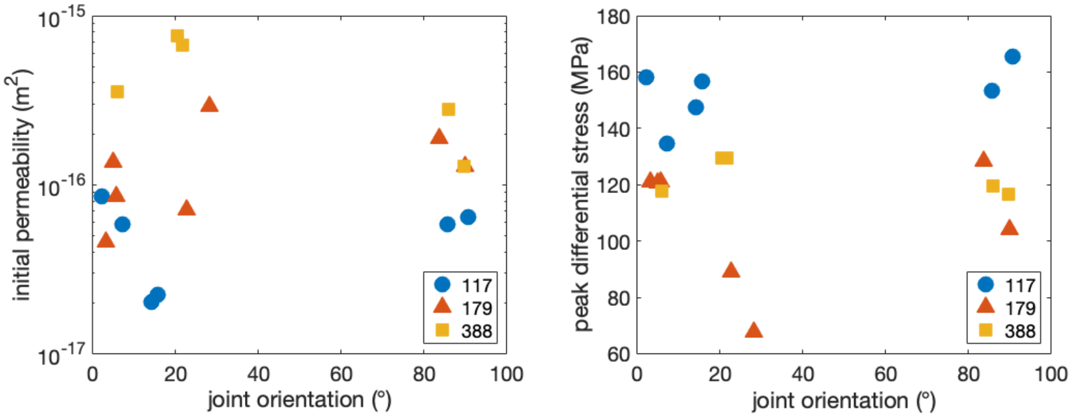

Permeability and peak differential stress of naturally joint buntsandstein.
Kushnir et al., in prep.

But how are these data used to understand the geothermal reservoir as a whole?

How are these laboratory data used in models?

Modelling regional fluid flow in the Upper Rhine Graben

(Vallier et al. 2018; 2019)

Property (unit)	Upper sediments	Lower sediments	Upper granites	Lower granites
Porosity, ϕ_o (%)	3.0[1]–35.0[1]	2.9[10]–20.7[11]	0.13[3]–25.55[3]	0.13[3]–0.8[1]
Total specific mass, r_0 (kg m^{-3})	2300[1]–2600[1]	2180[4]–2660[7]	2500[1]–2800[1]	2650[6]–2800[6]
Young's modulus, E (GPa)	10.0[1]–90.0[1]	8.0[1]–39.0[5]	25.0[9]–80.0[5]	25.0[9]–80.0[5]
Poisson's ratio, ν (–)	0.1[9]–0.33[1]	0.06[1]–0.46[1]	0.1[9]–0.38[5]	0.1[9]–0.38[5]
Biot coefficient, b (–)	0.65[1]–0.8[1]	0.8[1]–1.0[1]	0.27[1]–0.45[1]	0.27[1]–0.45[1]
Specific heat, c_s (J kg^{-1} K^{-1})	800[1]	800[1]	800[1]	800[1]
Thermal conductivity, λ_d (W m^{-1} K^{-1})	1.1[3]–5.9[3]	1.2[3]–4.2[3]	2.3[3]–4.3[3]	2.3[3]–4.3[3]
Thermal dilation, α_0 (10^{-5} K^{-1})	1.3[8]–1.5[8]	1.3[8]–1.5[8]	1.4[1]	1.4[1]
Heat source production, θ_{rad} (μ W m^{-3})	0.1[2]–1.0[3]	0.5[1]–1.0[3]	1.0[6]–6.2[5]	1.0[6]–6.2[5]
Permeability, K_{int} (m^2)	1.0×10^{-18}[4]–3.2×10^{-14}[4]	1.0×10^{-18}[11]–1.0×10^{-13}[10]	1.0×10^{-20}[12]–3.0×10^{-14}[12]	1.0×10^{-20}[12]–1.8×10^{-15}[3]

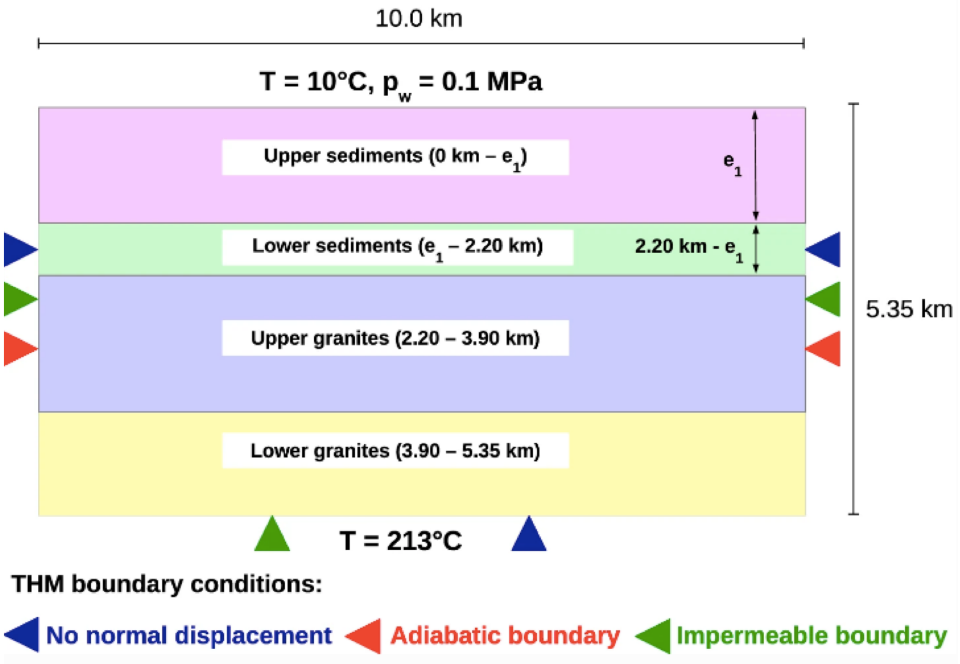

How are these laboratory data used in models?

Modelling chemical stimulation at Soultz-sous-Forêts

(Lucas et al. 2019)

Table 2
Main mineralogical composition, volume fraction and estimated reactive surface area of the matrix and facture Soultz granite considered in the current modelling work. The volume fraction values were taken from those in Jacquot (2000).

Minerals	Matrix		Fracture		
	Volume fraction (%)	Reactive surface area (m^2 $kg^{-1}H_2O$)	Minerals	Volume fraction (%)	Reactive surface area (m^2 $kg^{-1}H_2O$)
Quartz	24.2	288.40	Quartz	40.9	487.42
K-Feldspar	23.6	7777.20	K-Feldspar	13.9	4580.64
Albite	40.5	9231.49	Calcite	3.9	951.17
Anorthite	2	124.21	Mg-Illite	8.7	63757.49
Muscovite	3.13	701.22	Fe-Illite	8.7	66877.88
Annite	3.13	822.26	Al-Illite	8.7	66115.20
Phlogopite	3.13	691.15	Smectite	9.7	54841.96
Calcite	0.3	73.17	Dolomite	0.8	207.06
			Chamosite	2.4	137.19
			Clinochlore	2.4	107.86
Physical properties			**Physical properties**		
Porosity		10 %	Porosity		1 %
Permeability		10^{-16} m^2	Permeability		10^{-14} m^2

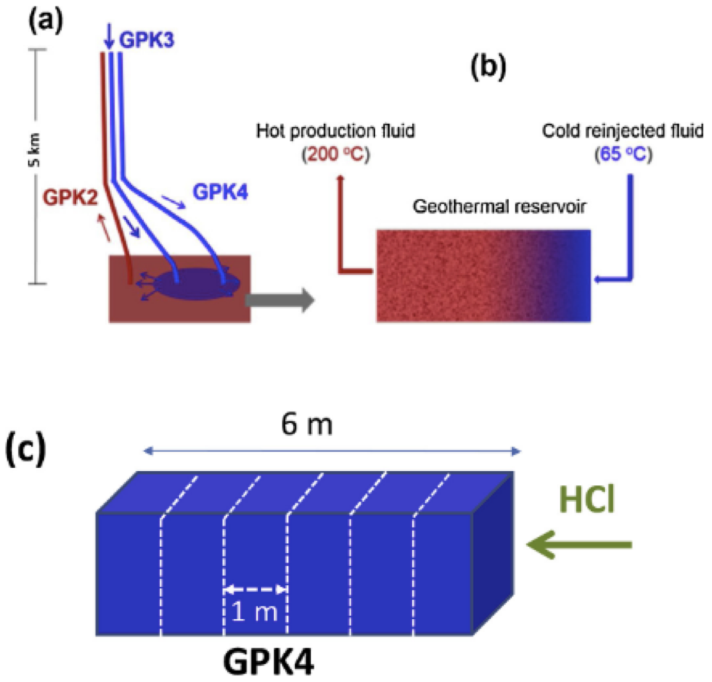

How are these laboratory data used in models?

Modelling hydraulic stimulation at Soultz-sous-Forêts

(AbuAisha et al. 2016)

Table 3
Material properties of Soultz-sous-Forêts reservoir as investigated by Evans et al. (2009). † The initial permeability is typical for granite (Taron and Elsworth, 2009).

Property	Value	Unit
Drained Young's modulus E	54	GPa
Drained Poisson's ratio ν	0.25	–
Bulk modulus of solid grains K_s	50	GPa
Bulk modulus of fluid K_f	2.2	GPa
Dynamic viscosity of fluid μ	3×10^{-4}	Pa × s
Porosity ϕ_0	0.1003	–
Initial permeability† k_0	6.8×10^{-15}	m^2
Solid thermal conductivity $k_{\theta s}$	2.49	W/m/K
Fluid thermal conductivity $k_{\theta f}$	0.6	W/m/K
Solid heat capacity at constant volume c_{vs}	1000	J/kg/K
Fluid heat capacity at constant volume c_{vf}	4200	J/kg/K
Density of solid ρ_s	2910.2	kg/m^3
Unit weight of water γ_f	9800	N/m^3
Cubical thermal expansion of the solid α_s	7.5×10^{-6}	K^{-1}
Cubical thermal expansion of the fluid α_f	1×10^{-3}	K^{-1}

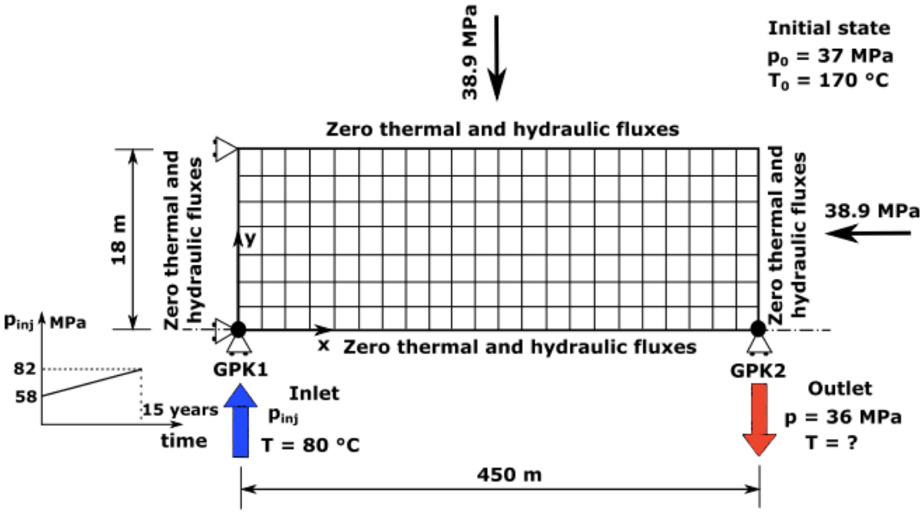

Are the physical properties used representative of the reservoir?

Often these values don't take into account large-scale fractures.

Soultz-sous-Forêts: A fractured reservoir

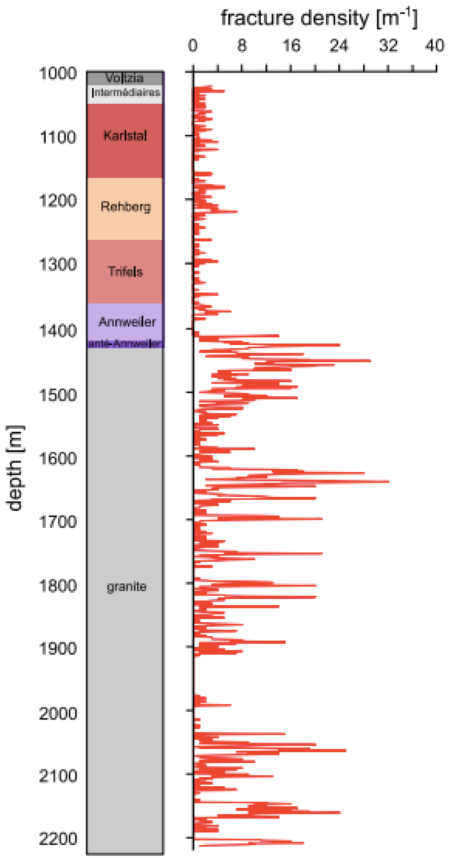

Heap et al. 2019

The Soultz-sous-Forêts geothermal reservoir is fractured.

These fractures are not easily accounted for on the scale of laboratory samples.

But fractures have a significant effect on:

- Permeability
- Rock strength

Case study 1:

Scaling permeability

Kushnir, A. R.L., Heap, M. J., & Baud, P. (2018). Assessing the role of fractures on the permeability of the Permo-Triassic sandstones at the Soultz-sous-Forêts (France) geothermal site. Geothermics, 74, 181-189.

Scaling permeability to the borehole:

Defining equivalent permeability

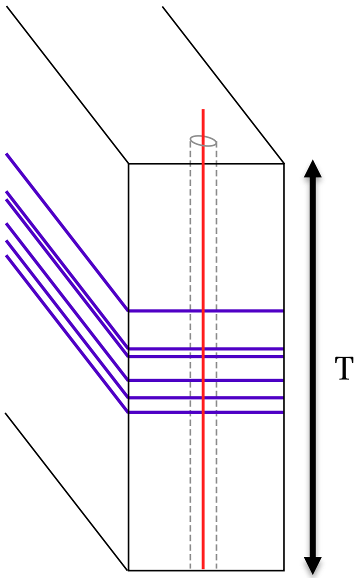

Consider a volume of rock of thickness, T.

The **equivalent permeability**, $\mathbf{k_e}$, of the rock unit can be calculated:

$$k_e = \frac{w_i k_i + w_f k_f}{T}$$

k_e – equivalent permeability
w_i – width of the intact rock
k_i – permearbility of the intact rock
w_f – total width of fractures
k_f – fracture permeability
T – total thickness of the rock unit

Using borehole televiewer, we can characterise:

- fracture density
- fracture aperture

In the lab, we can characterise:

- matrix permeability, k_i
- fracture permeability, k_f

What happens in the lab?

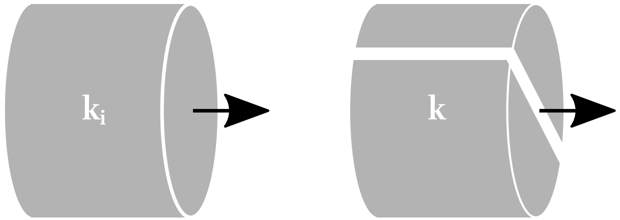

Cylindrical samples: **25 mm x 25 mm**

Connected porosity (φ): measured using helium pycnometry

Gas permeability (k_i and k): measured using a bench-top permeameter using either the **steady state flow** or **pulse decay** methods.

Procedure:

1. Measure the permeability of the intact material.

2. Fracture the sample in the lab using a Brazil test configuration.

3. Measure the permeability of the fractured material.

Permeability before and after fracture

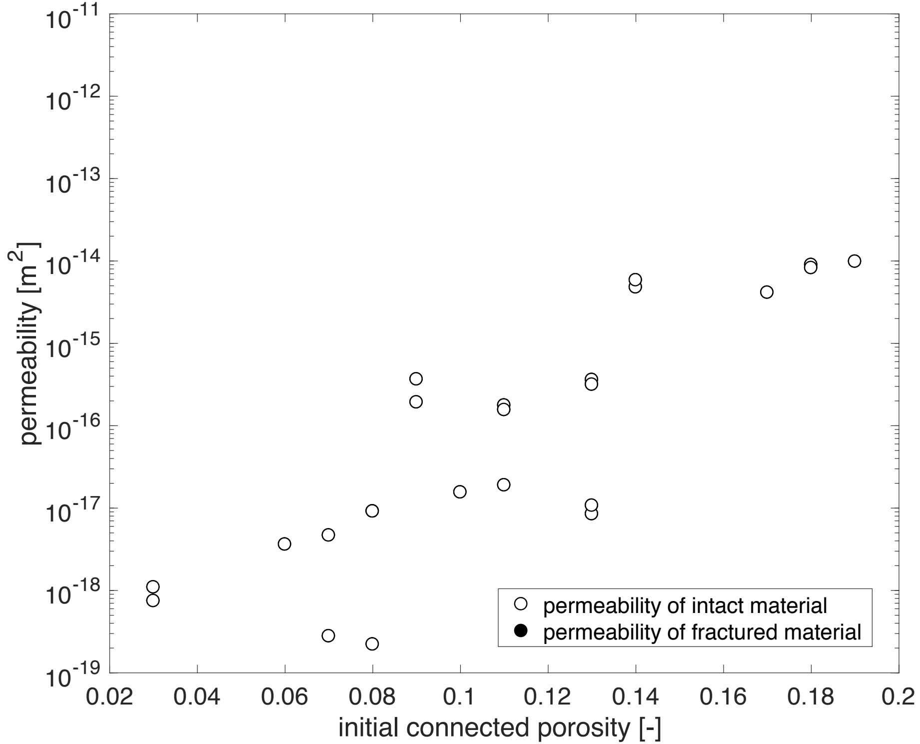

Intact material:

$2 \times 10^{-19} < k_i < 1 \times 10^{-14}\ m^2$

$0.03 < \varphi < 0.19$

Permeability varies over **5 orders** of magnitude.

Permeability before and after fracture

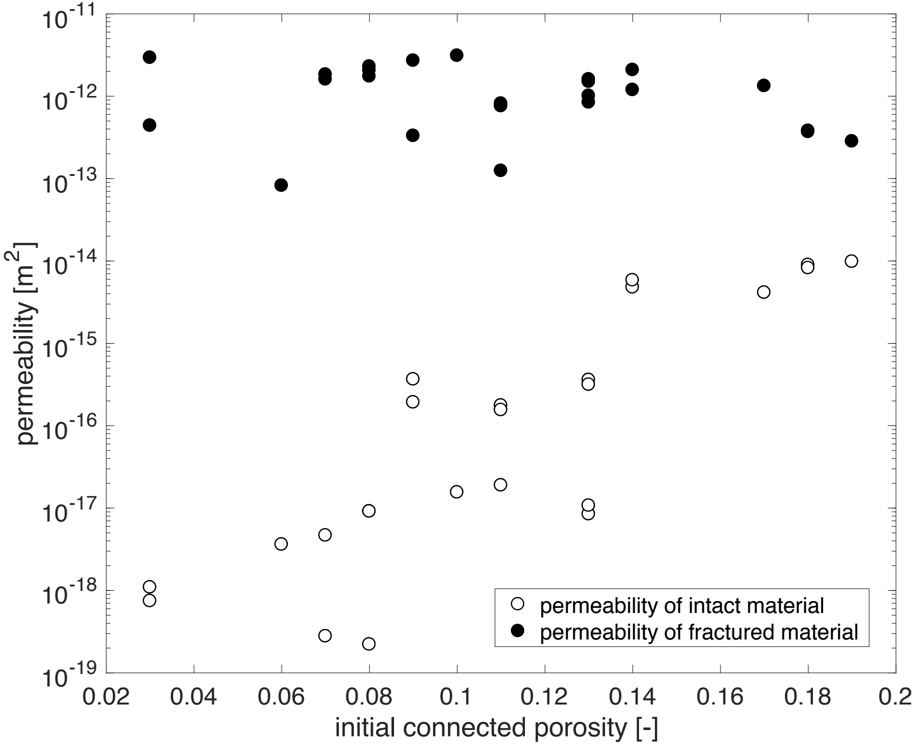

Fractured material:

$8 \times 10^{-14} < k < 3 \times 10^{-12}$ m^2

Permeability varies over **2 orders** of magnitude.

Permeability increased by up to **6 orders** of magnitude

Fracture widths between 0.2 and 1 mm

What happens in the lab?

The permeability of the fracture can be calculated:

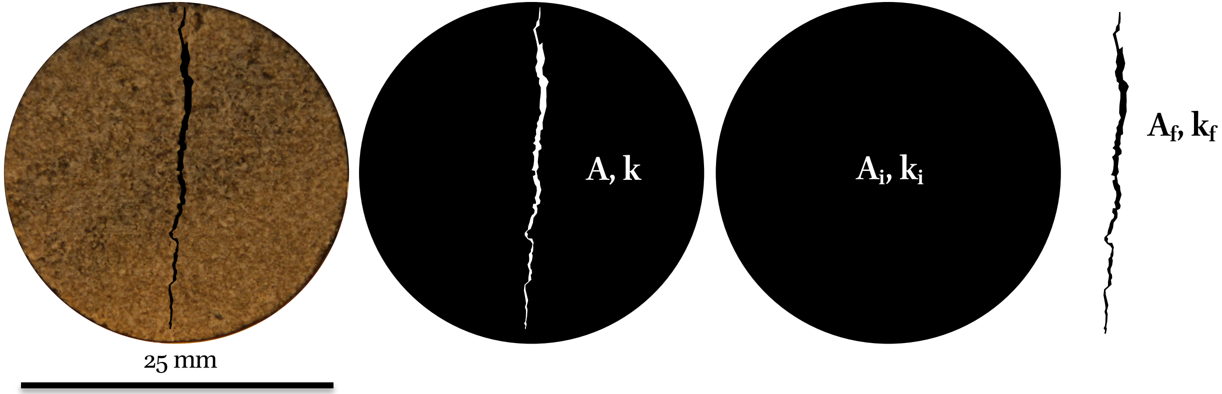

$$k_f = \frac{Ak - A_i k_i}{A_f}$$

Where:
k_f – fracture permeability
A_f – cross-sectional area of the fracture
k_i – permearbility of the intact sample
A_i – cross-sectional area of the intact sample
k – permeability of the fractured sample
A – cross-sectional area of the fractured sample

Fracture permeability: $1 \times 10^{-11} < k_f < 1 \times 10^{-10}$ m^2

From the laboratory to the borehole

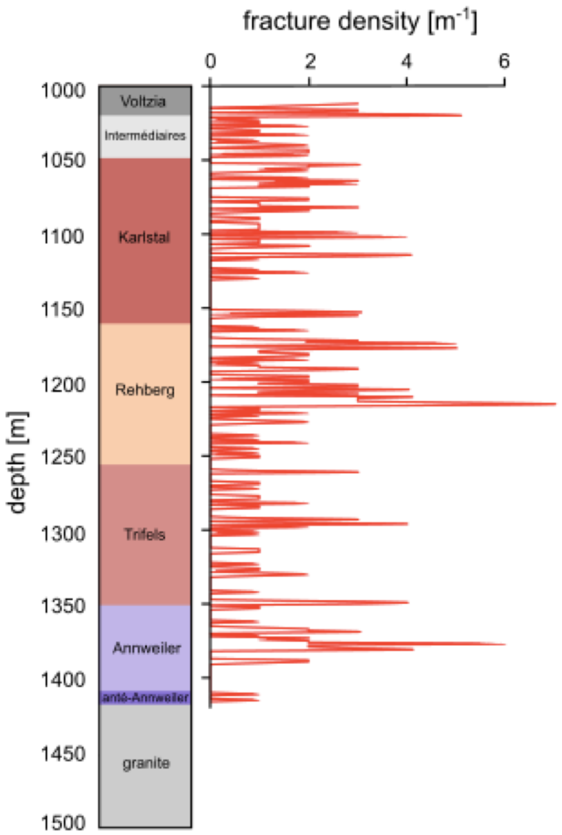

Heap et al. 2019

We can calculate the equivalent permeability of a rock mass because we know:

- Fracture density
- Fracture width
- Degree of fracture filling

- Permeability if the intact material $2 \times 10^{-19} < k_i < 1 \times 10^{-14}$ m²
- Permeability of the fractures $1 \times 10^{-11} < k_f < 1 \times 10^{-10}$ m²

$$k_e = \frac{w_i k_i - w_f k_f}{T}$$

k_e – equivalent permeability
w_i – width of the intact rock
k_i – permearbility of the intact rock
w_f – total width of fractures
k_f – fracture permeability
T – total thickness of the rock unit

Equivalent permeability with depth

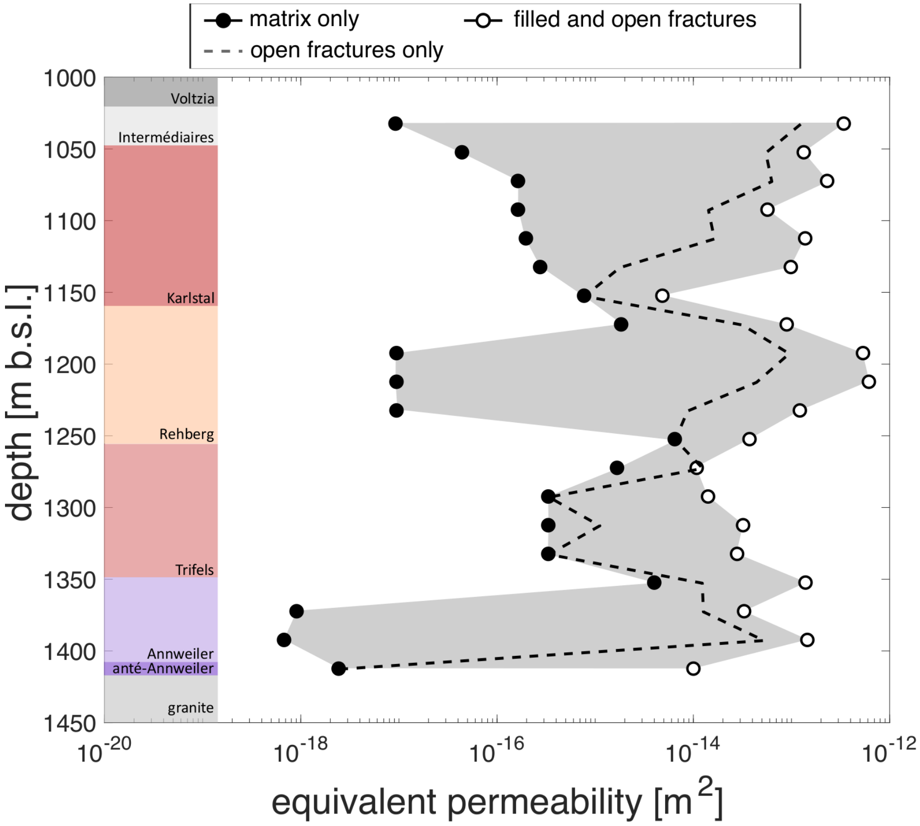

Data binned every 20 m.

Average matrix permeability down the borehole:
$7 \times 10^{-19} < k_e < 7 \times 10^{-15}$ m².

When **all** fractures are open:
$5 \times 10^{-15} < k_e < 6 \times 10^{-13}$ m².

Consider fracture fill to have a permeability of 0 m².

80% of fractures filled:
$2 \times 10^{-18} < k_e < 1 \times 10^{-13}$ m²

Equivalent permeability with depth

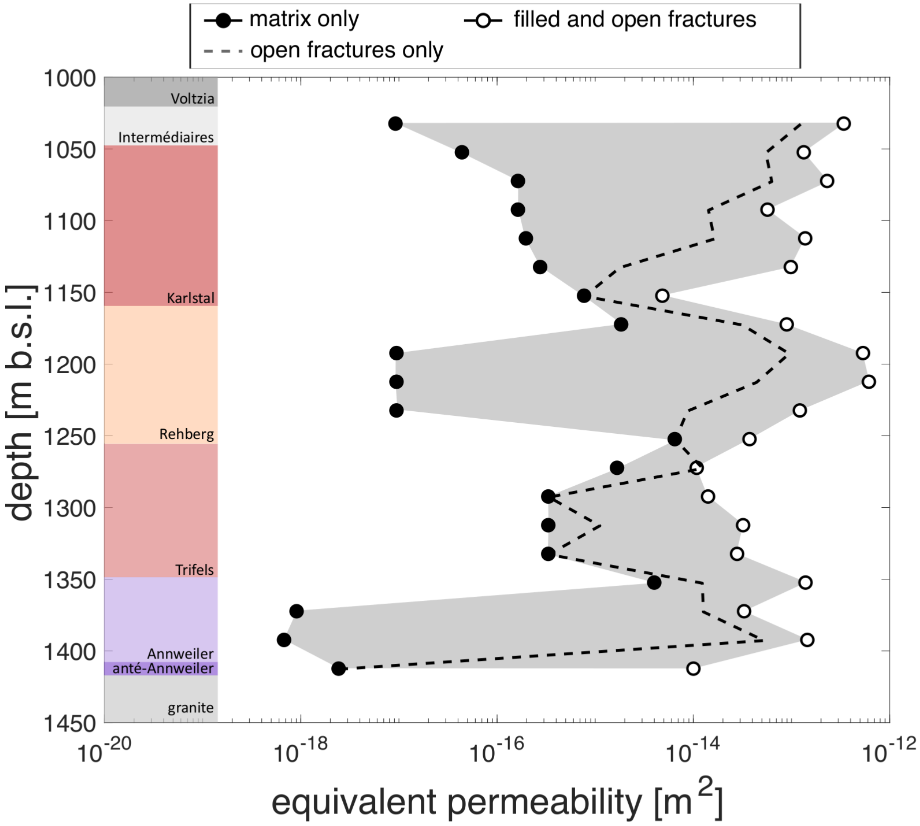

These values are consistent with hydraulic conductivity data for the Bundsandstein (from Stober and Bucher, 2015)

These values are the most appropriate to use in large scale models

Case study 2:

Scaling rock strength

Villeneuve, M. C., Heap, M. J., Kushnir, A. R., Qin, T., Baud, P., Zhou, G., & Xu, T. (2018). Estimating in situ rock mass strength and elastic modulus of granite from the Soultz-sous-Forêts geothermal reservoir (France). Geothermal Energy, 6(1), 11.

Heap, M. J., Villeneuve, M., Kushnir, A. R., Farquharson, J. I., Baud, P., & Reuschlé, T. (2019b). Rock mass strength and elastic modulus of the Buntsandstein: an important lithostratigraphic unit for geothermal exploitation in the Upper Rhine Graben. Geothermics, 77, 236-256.

What happens in the lab?

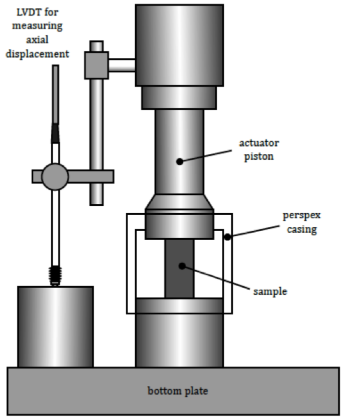

Heap et al. 2020

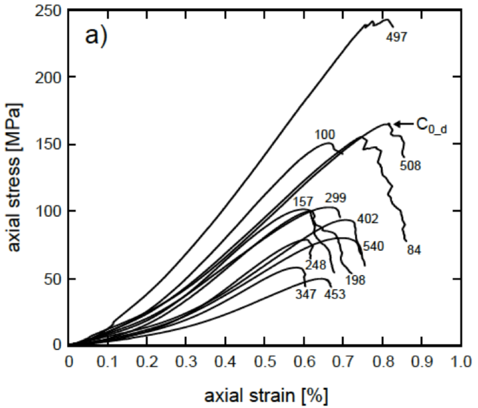

Buntsandstein

Heap et al. 2019

In the laboratory we can perform:

- Uniaxial compressive strength (UCS) measurements
- triaxial deformation experiments

Cylindrical samples: **20 mm x 40 mm**

These experiments do not take larger fractures into account, which we know greatly influence strength

Generalised Hoek-Brown failure criterion

$$\sigma_1' = \sigma_3' + C_o\left(m_b\frac{\sigma_3'}{C_o} + s\right)^a$$

$$m_b = m_i\, e^{\left(\frac{GSI-100}{28-14D}\right)}$$

$$s = e^{\left(\frac{GSI-100}{9-3D}\right)}$$

$$a = \frac{1}{2} + \frac{1}{6}\left(e^{-\frac{GSI}{15}} + e^{\frac{-20}{3}}\right)$$

$\boldsymbol{\sigma}_1$' – maximum principal stress (MPa)
$\boldsymbol{\sigma}_3$ ' – minimum principal stress (MPa)
C_o – uniaxial compressive strengh (MPa)
m_i – unitless empirical fitting parameter related to lithology (Eberhardt, 2012)
GSI – geological strength index (Marinos et al., 2005)
D – damage factor, 0 for when there is no blast damage

Hoek et al. 2002

An empirical expression that characterizes **rock mass strength**.

Suggested ISRM method.

Accounts for the lower strength of fractured rock masses.

Generalised Hoek-Brown failure criterion

$$\sigma_1' = \sigma_3' + C_o \left(m_b \frac{\sigma_3'}{C_o} + s \right)^a$$

$$m_b = m_i \, e^{\left(\frac{GSI-100}{28-14D}\right)}$$

$$s = e^{\left(\frac{GSI-100}{9-3D}\right)}$$

$$a = \frac{1}{2} + \frac{1}{6}\left(e^{-\frac{GSI}{15}} + e^{\frac{-20}{3}}\right)$$

$\boldsymbol{\sigma}_1$' – maximum principal stress (MPa)

$\boxed{\boldsymbol{\sigma}_3\text{' – minimum principal stress (MPa)}}$

C_o – uniaxial compressive strengh (MPa)

m_i – unitless empirical fitting parameter related to lithology (Eberhardt, 2012)

GSI – geological strength index (Marinos et al., 2005)

D – damage factor, 0 for when there is no blast damage

For the Soutlz-sous-Forêts reservoir:

$$\boldsymbol{\sigma}_3' = S_{hmin} = 0.0130z,$$

where z is depth in meters, Evans 2005

Generalised Hoek-Brown failure criterion

$$\sigma_1' = \sigma_3' + C_o\left(m_b \frac{\sigma_3'}{C_o} + s\right)^a$$

$$m_b = m_i\, e^{\left(\frac{GSI-100}{28-14D}\right)}$$

$$s = e^{\left(\frac{GSI-100}{9-3D}\right)}$$

$$a = \frac{1}{2} + \frac{1}{6}\left(e^{-\frac{GSI}{15}} + e^{\frac{-20}{3}}\right)$$

$\boldsymbol{\sigma}_1$' – maximum principal stress (MPa)
$\boldsymbol{\sigma}_3$' – minimum principal stress (MPa)
C_o – uniaxial compressive strengh (MPa)
m_i – unitless empirical fitting parameter related to lithology (Eberhardt, 2012)
GSI – geological strength index (Marinos et al., 2005)
D – damage factor, 0 for when there is no blast damage

<u>C_o and m_i can be determined in the lab:</u>

C_o – uniaxial compressive stress (MPa) at 10^{-5} s^{-1}

m_i – describes the shape of the failure envelope, triaxial experiments at 10^{-5} s^{-1}, calculated in RocData (Rocscience Inc, 2017)

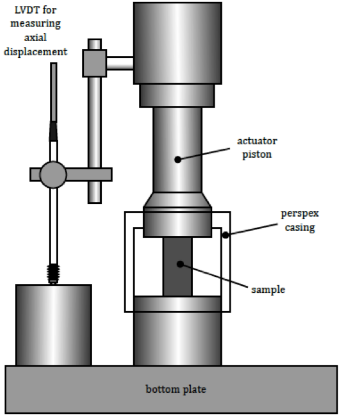

Heap et al. 2020

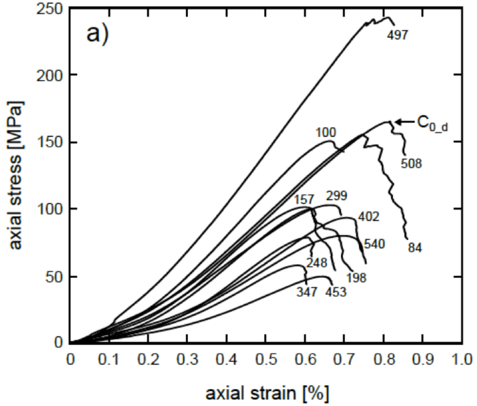

Buntsandstein
Heap et al. 2019

Generalised Hoek-Brown failure criterion

$$\sigma_1' = \sigma_3' + C_o\left(m_b \frac{\sigma_3'}{C_o} + s\right)^a$$

$$m_b = m_i\, e^{\left(\frac{GSI-100}{28-14D}\right)}$$

$$s = e^{\left(\frac{GSI-100}{9-3D}\right)}$$

$$a = \frac{1}{2} + \frac{1}{6}\left(e^{-\frac{GSI}{15}} + e^{\frac{-20}{3}}\right)$$

$\boldsymbol{\sigma}_1$' – maximum principal stress (MPa)
$\boldsymbol{\sigma}_3$' – minimum principal stress (MPa)
C_o – uniaxial compressive strengh (MPa)
m_i – unitless empirical fitting parameter related to lithology (Eberhardt, 2012)
GSI – geological strength index (Marinos et al., 2005)
D – damage factor, 0 for when there is no blast damage

C_o and m_i can be determined in the lab:

C_o – uniaxial compressive stress (MPa) at 10^{-5} s^{-1}

m_i – describes the shape of the failure envelope, triaxial experiments at 10^{-5} s^{-1}, calculated in RocData (Rocscience Inc, 2017)

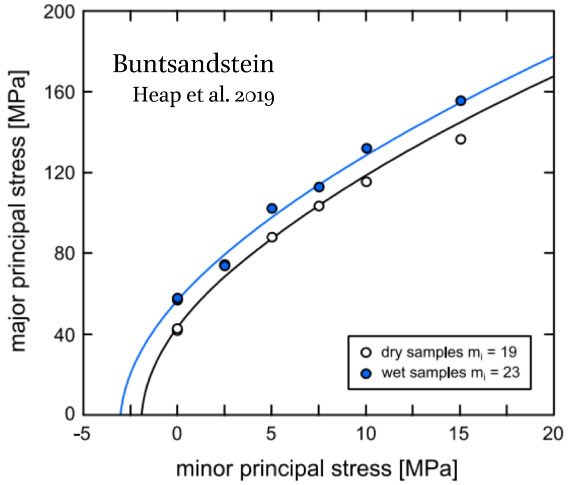

Generalised Hoek-Brown failure criterion

$$\sigma_1' = \sigma_3' + C_o\left(m_b\frac{\sigma_3'}{C_o} + s\right)^a$$

$$m_b = m_i\, e^{\left(\frac{GSI-100}{28-14D}\right)}$$

$$s = e^{\left(\frac{GSI-100}{9-3D}\right)}$$

$$a = \frac{1}{2} + \frac{1}{6}\left(e^{\frac{-GSI}{15}} + e^{\frac{-20}{3}}\right)$$

σ_1' – maximum principal stress (MPa)
σ_3' – minimum principal stress (MPa)
C_o – uniaxial compressive strengh (MPa)
m_i – unitless empirical fitting parameter related to lithology (Eberhardt, 2012)
GSI – geological strength index (Marinos et al., 2005)
D – damage factor, 0 for when there is no blast damage

What we can determine from the core:

GSI is a dimensionless parameter that combines rock mass structure (e.g. fracture density) and fracture quality (e.g. weathering or infilling)

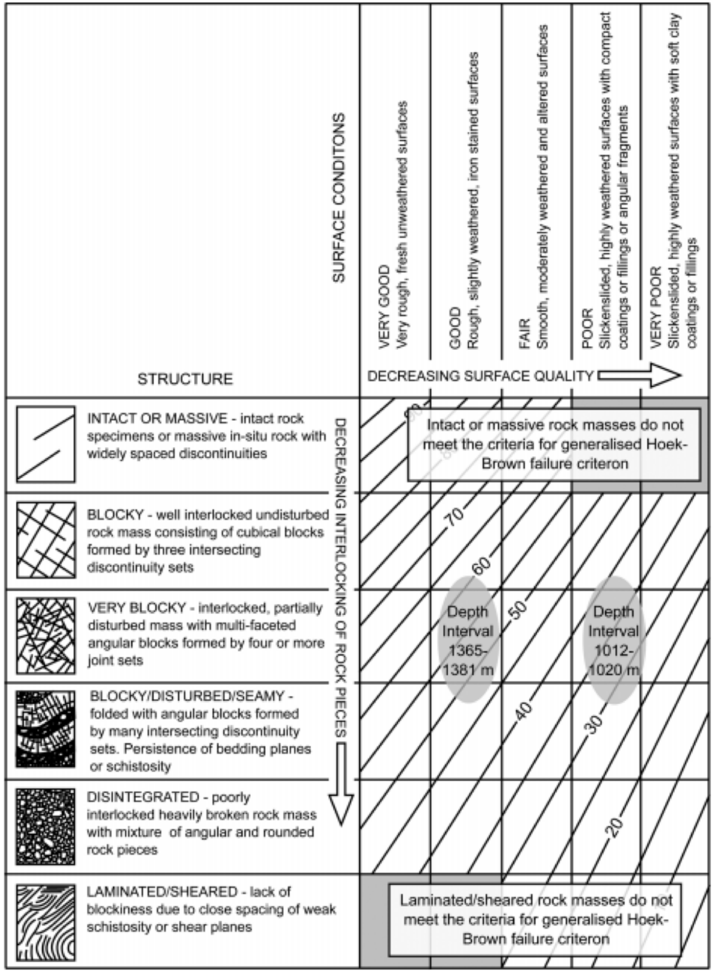

Marinos et al. 2005

Upscaled strength down EPS-1

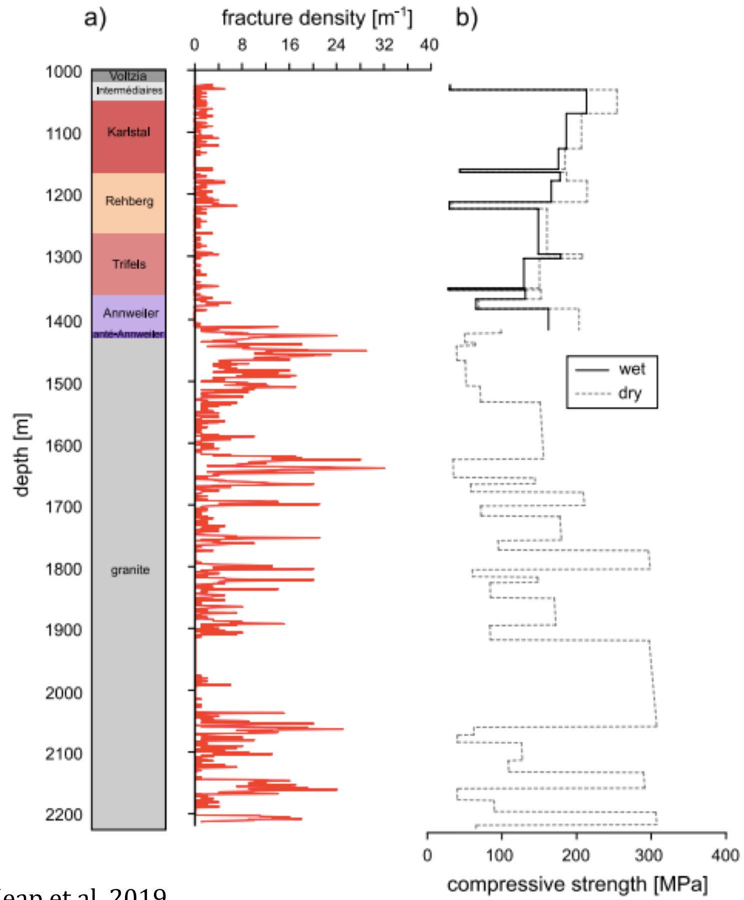

Heap et al. 2019

Takes into account:

- the strengthening of rock as a function of pressure
- the weakening influence of fractures

These values are at a scale appropriate for large scale modelling

The role of rock physics in geothermal energy

Rock properties are needed for large scale geothermal models.

The more representative these values are, the better the results of the model.

Laboratory values are not ideal – they ignore large fractures that we know influence rock properties.

Laboratory measurements can be upscaled, with the help of complimentary geological information, including borehole logs.

References

AbuAisha, M., Loret, B., & Eaton, D. (2016). Enhanced Geothermal Systems (EGS): Hydraulic fracturing in a thermo-poroelastic framework. Journal of Petroleum Science and Engineering, 146, 1179-1191.

Baillieux, P., Schill, E., Edel, J. B., & Mauri, G. (2013). Localization of temperature anomalies in the Upper Rhine Graben: insights from geophysics and neotectonic activity. *International Geology Review*, *55*(14), 1744-1762.

Evans, K. F., Moriya, H., Niitsuma, H., Jones, R. H., Phillips, W. S., Genter, A., ... & Baria, R. (2005). Microseismicity and permeability enhancement of hydrogeologic structures during massive fluid injections into granite at 3 km depth at the Soultz HDR site. *Geophysical Journal International*, *160*(1), 388-412.

Farquharson, J. I., Kushnir, A. R., Wild, B., & Baud, P. (2020). Physical property evolution of granite during experimental chemical stimulation. *Geothermal Energy*, *8*(1), 1-24.

Heap, M. J., Kushnir, A. R., Gilg, H. A., Wadsworth, F. B., Reuschlé, T., & Baud, P. (2017). Microstructural and petrophysical properties of the Permo-Triassic sandstones (Buntsandstein) from the Soultz-sous-Forêts geothermal site (France). Geothermal Energy, 5(1), 26.

Heap, M. J., Reuschlé, T., Kushnir, A. R., & Baud, P. (2018). The influence of hydrothermal brine on the short-term strength and elastic modulus of sandstones from exploration well EPS-1 at Soultz-sous-Forêts (France). Geothermal Energy, 6(1), 29.

Heap, M. J., Villeneuve, M., Kushnir, A. R., Farquharson, J. I., Baud, P., & Reuschlé, T. (2019). Rock mass strength and elastic modulus of the Buntsandstein: an important lithostratigraphic unit for geothermal exploitation in the Upper Rhine Graben. Geothermics, 77, 236-256.

Heap, M. J., Villeneuve, M., Albino, F., Farquharson, J. I., Brothelande, E., Amelung, F., ... & Baud, P. (2020). Towards more realistic values of elastic moduli for volcano modelling. *Journal of Volcanology and Geothermal Research*, *390*, 106684.

References

Hoek, E., Carranza-Torres, C., & Corkum, B. (2002). Hoek-Brown failure criterion-2002 edition. *Proceedings of NARMS-Tac*, *1*(1), 267-273.

Kushnir, A. R., Heap, M. J., & Baud, P. (2018). Assessing the role of fractures on the permeability of the Permo-Triassic sandstones at the Soultz-sous-Forêts (France) geothermal site. Geothermics, 74, 181-189.

Lucas, Y., Ngo, V. V., Clément, A., Fritz, B., & Schäfer, G. (2020). Modelling acid stimulation in the enhanced geothermal system of Soultz-sous-Forêts (Alsace, France). Geothermics, 85, 101772.

Marinos, V. I. I. I., Marinos, P., & Hoek, E. (2005). The geological strength index: applications and limitations. *Bulletin of Engineering Geology and the Environment*, *64*(1), 55-65.

Stober, I., & Bucher, K. (2015). Hydraulic conductivity of fractured upper crust: insights from hydraulic tests in boreholes and fluid-rock interaction in crystalline basement rocks. *Geofluids*, *15*(1-2), 161-178.

Vallier, B., Magnenet, V., Schmittbuhl, J., & Fond, C. (2018). THM modeling of hydrothermal circulation at Rittershoffen geothermal site, France. Geothermal Energy, 6(1), 22.

Vallier, B., Magnenet, V., Schmittbuhl, J., & Fond, C. (2019). Large scale hydro-thermal circulation in the deep geothermal reservoir of Soultz-sous-Forêts (France). Geothermics, 78, 154-169.

Vidal, J., Genter, A., & Schmittbuhl, J. (2015). How do permeable fractures in the Triassic sediments of Northern Alsace characterize the top of hydrothermal convective cells? Evidence from Soultz geothermal boreholes (France). *Geothermal Energy*, *3*(1), 1-28.

Villeneuve, M. C., Heap, M. J., Kushnir, A. R., Qin, T., Baud, P., Zhou, G., & Xu, T. (2018). Estimating in situ rock mass strength and elastic modulus of granite from the Soultz-sous-Forêts geothermal reservoir (France). Geothermal Energy, 6(1), 11.